Materials Advances

ROYAL SOCIETY OF CHEMISTRY

PAPER

View Article Online
View Journal | View Issue

Cite this: *Mater. Adv.*, 2024, 5, 7766

Stripping analysis of Pb^{2+} and Hg^{2+} in deveined shrimp and eggshells using a H_2bpabza/MWCNT–modified graphite electrode

Kumar Sangeetha Selvan, *[a] Jayagopi Gayathri *[b] and Sivakumar Sivalingam [b]

A novel synthesis was performed of asymmetrical carboxamide ligand *N*,*N*′-bis(2-pyridinecarboxamide)-2-aminobenzylamine (H_2bpabza) derived from 2-pyridinecarboxylic acid and 2-aminobenzylamine. The *N*,*N*′-bis(2-pyridinecarboxamide)-2-aminobenzylamine (H_2bpabza) ligand was confirmed by ultraviolet-Visible (UV-Vis), Fourier transform infrared (FT-IR), and Raman spectroscopy. The fabrication of *N*,*N*′-bis(2-pyridinecarboxamide)-2-aminobenzylamine (H_2bpabza) embedded in a multi-walled carbon nanotube (MWCNT)-modified graphite electrode (GE) for use as an electrochemical sensor of Pb^{2+} and Hg^{2+} was demonstrated. The performance of the H_2bpabza/MWCNT electrode and (Pb^{2+} and Hg^{2+}–H_2bpabza)/MWCNT was investigated by scanning electron microscopy (SEM) and square wave anodic stripping voltammetry (SWASV). In comparison to the MWCNT electrode, the H_2bpabza/MWCNT electrode exhibited higher sensitivity and conductivity, as determined by cyclic voltammetry (CV) and electrochemical impedance spectroscopy (EIS). Stripping analysis and detailed experiments were conducted to establish the optimal parameters for deposition and stripping of metal ions, such as supporting electrolytes, pH, and accumulation time. The linear range was 2 to 140 μg L^{-1}, with a detection limit of 0.1 μg L^{-1} for Pb^{2+} and 0.3 μg L^{-1} for Hg^{2+} (S/N = 3). The H_2bpabza/MWCNT-modified GE showed excellent sensitivity, selectivity, stability, and reproducibility for the determination of Pb^{2+} and Hg^{2+}. Ultimately, the H_2bpabza/MWCNT-modified GE was used to demonstrate the electrochemical sensing of Pb^{2+} and Hg^{2+} in deveined shrimp and eggshells.

Received 30th March 2024,
Accepted 27th August 2024

DOI: 10.1039/d4ma00335g

rsc.li/materials-advances

1. Introduction

It is well known that heavy metal ions (HMIs) such as those from lead and mercury are extremely hazardous environmental pollutants with toxic effects on living organisms.[1–3] Trace amounts of lead and mercury enter the body primarily through inhalation and ingestion, and this damages many of the body's organ systems, *e.g.*, the brain, lungs, and kidney.[4,5] Although mercury is not an abundant chemical element in nature, it has become widespread as a result of its presence in many industrial and agricultural applications.[6–8] Therefore, detection is important, and sensor performance has previously been investigated in the determination of lead and mercury in different food samples.[9–11] Consequently, there has been considerable development of new methods for the detection of lead and mercury and at low or innocuous levels because of the potential for widespread practical applications for such technology.

Traditionally, the presence of lead and mercury ions has been determined using spectroscopic methods such as inductively coupled plasma mass spectrometry (ICP-MS),[12,13] inductively coupled plasma optical emission spectrometry (ICP-OES),[14,15] atomic absorption spectrometry (AAS),[16,17] and atomic fluorescence spectrometry (AFS).[18–21] Although these methods have been developed for trace metal determination, unfortunately, these techniques require expensive instruments with high operating costs, and they are not suitable for on-site analysis.[22] Among the different analytical methods, electrochemical techniques are an alternative to conventional spectroscopic techniques, and have been recognized as promising methods for trace and on-site analysis of toxic heavy metal ions due to their excellent sensitivity, portability, low cost, and suitability.[23] Among all the electrochemical methods, anodic stripping voltammetry (ASV) is a powerful tool for detection of mercury and lead ions because it possesses high sensitivity and has the ability to simultaneously analyze several trace metal ions.[24–27]

There has been considerable academic and industrial research on multiwalled carbon nanotubes (MWCNTs) due to

[a] *Department of Chemistry, Anna Adarsh College for Women, Anna Nagar, Chennai, Tamil Nadu 600040, India. E-mail: msc.sangi@gmail.com*
[b] *Department of Chemistry, Vel Tech Rangarajan Dr Sagunthala R & D Institute of Science and Technology, Avadi, Chennai, Tamil Nadu 600062, India. E-mail: drgayathrij@veltech.edu.in, drsivakumars@veltech.edu.in*

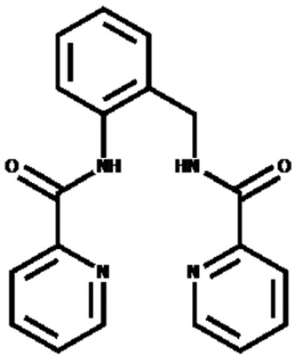

Scheme 1 *N,N′*-Bis(2-pyridinecarboxamide)-2-aminobenzylamine (H_2bpabza).

their excellent electrical properties, and when incorporated into graphite, high-performance conductivity and stability results. When graphite electrodes (GEs) are incorporated into sensor applications, they enhance the contact with the metal and improve the electron transfer charges to increase the sensitivity and selectivity of the electrode.

The important aspect in chemically modified electrodes (CMEs) is the choice of the modifier, which confers unique characteristics to the electrode surface.[28–31] Asymmetric Schiff base ligand was chosen as the modifier in this work because it readily complexes with transition metal ions such as mercury, lead, and cadmium. Schiff base ligands play a key role as chelating agents in main group and transition metal coordination chemistry, due to the ease of synthesis, their role in biological systems, and diverse therapeutic activities.[32–35] Carboxamide ligand was chosen as the modifier in this work because it readily complexes with transition metal ions such as lead and mercury. The structure of the ligand is given below in Scheme 1.

In this work, a carboxamide ligand was synthesized according to the protocol by Meghdadi *et al.*,[36] which described a reaction between 2-pyridinecarboxylic acid and 2-aminobenzylamine, in tetrabutylammonium bromide medium with triphenyl phosphite as the activator. The MWCNT/ligand was coated on the electrode by the drop-casting method to fabricate a mercury-free electrode for the anodic stripping voltammetric determination of Pb^{2+} and Hg^{2+}. In this study, the ligand was used for the first time as a sensing material on the surface of an electrode. This modified electrode was applied for the simultaneous determination of Pb^{2+} and Hg^{2+} in solution by square wave anodic stripping voltammetry (SWASV). The modified electrode displayed higher peak current responses for lead and cadmium as compared to the bare electrode. The modified platform exhibits satisfactory electrochemical stability and reusability.

2. Experimental

2.1. Materials and instruments

A solution of 0.1 M acetate buffer (ABS) was prepared using sodium acetate and acetic acid with double-distilled water (DDW). All reagents, 2-pyridinecarboxylic acid, 2-aminobenzylamine, tetrabutylammonium bromide (TBAB), and triphenyl phosphite (TPP) were purchased from Sigma-Aldrich and used without further purification. Stock solutions of lead acetate and cadmium acetate (1 mM) were prepared using DDW in standard flasks. Raman spectroscopy was performed using an inVia Raman microscope with a Raman-11i high-resolution confocal Raman microscope (Nanophoton, Japan), and UV-Visible spectroscopy was performed with a Cary 8453 UV-Vis diode array spectrophotometer. FTIR was carried out using a Cary 630 FTIR spectrometer. All electrochemical measurements were performed using a CHI 660B potentiostat, (CH Instruments, USA). A conventional three-electrode system was used that consisted of the Schiff base ligand/MWCNT-modified electrode as the working electrode (3-mm diameter), a platinum electrode as the auxiliary electrode, and an Ag/AgCl electrode saturated by KCl as the reference electrode. Solutions were mixed on a magnetic stirrer during purging with high-purity nitrogen, and were preconcentrated with a rotating PTFE stir bar.

2.2. Synthesis of *N,N′*-bis(2-pyridinecarboxamide)-2-aminobenzylamine (H_2bpabza) ligand

The preparation of carboxamide ligand was carried out as previously reported[36] with slight modification. In brief, (10 mmol) 3.1 g triphenyl phosphite (TPP), (5 mmol) 1.61 g tetrabutylammonium bromide (TBAB), (10 mmol) 1.231 g 2-pyridinecarboxylic acid, and (5 mmol) 0.611 g 2-aminobenzylamine were placed in a 25-mL round bottom flask and heated in an oil bath. The reaction mixture was vigorously stirred for 20 min at 120 °C and then heated until a viscous and homogeneous solution was formed. The resulting viscous solution was cooled to room temperature, and then, 10 mL of methanol was added, and a clear solution was obtained by stirring. The solution was dried under vacuum for 24 h to obtain white crystals of the ligand.

2.3. Fabrication of H_2bpabza/MWCNT/PGE

Paraffin-impregnated graphite electrodes (PGEs) 4 cm in length with a diameter of 3 mm were used for modification. The PGEs were prepared as previously reported[37] by immersing graphite rods into molten wax under vacuum until air bubbles ceased to evolve from the rods. After re-establishing atmospheric pressure, the graphite rods were removed before the solidification of the paraffin. The PGEs were then polished to a mirror-like finish by rubbing over the finest grade of emery paper, and the polished surface was washed thoroughly with DDW. Next, 5 μL (0.1 mg) of MWCNTs dispersed in 1 mL of ethanol was coated on the polished PGE surface and allowed to dry. Then, carboxamide ligand, which was dissolved in acetonitrile and 5 μL (1 mM) of carboxamide ligand, was drop-cast onto the MWCNT electrode surface, allowed to dry, and then washed with distilled water.

2.4. Stripping voltammetry with the H_2bpabza/MWCNT-modified electrode for Pb^{2+} and Hg^{2+} determination

The anodic stripping voltammetric determination of Pb^{2+} and Hg^{2+} was carried out in the following manner. The H_2bpabza/MWCNT-modified electrode was immersed in a known amount

of solution containing Pb^{2+} and Hg^{2+} present in 60 mL of 0.1 M acetate buffer solution (pH 4.5), and stirred for 180 s. Then, the modified electrode was removed, washed, and stored in fresh acetate buffer solution. Applying the negative potential of −0.8 V implies that the metal ions deposited on the electrode surface were reduced. The reduction of metal ion (Pb^{2+} and Hg^{2+}) to metal (Pb^{0} and Hg^{0}) on the electrode surface was determined by scanning the potential range from −0.8 V to 0.6 V, and the amplitude and the potential steps were 25 mV and 4 mV, respectively.

2.5. Preparation of deveined shrimp and eggshells

Deveined shrimp (sample A) and eggshells (sample B) were collected from a fish market and egg shop in Chennai (India). Both samples were repeatedly washed with DDW, and then subsequently heated at 80 °C in an air oven for 1 hour. The dried samples of deveined shrimp and eggshells were separately powdered for further studies. 0.1 mM of $Pb^{2+}$and Hg^{2+} was added to a freshly prepared stock solution of deveined shrimp and eggshell, and these samples were subsequently used to detect $Pb^{2+}$and Hg^{2+} by SWASV.

3. Results and discussion

3.1. Characterization of the H_2bpabza ligand

3.1.1 UV-Visible spectroscopy. The UV-Visible absorption spectrum of the ligand is shown in Fig. 1. Two absorption peaks at 218 and 286 nm were seen for the ligand, and a shoulder at 330 nm was assigned to the π–π* transitions of the aromatic rings in the UV range. No absorption peak was observed for the ligand in the visible region.

3.1.2 FT-IR spectroscopy. The FT-IR spectrum of the asymmetric ligand is shown in Fig. 2. The IR spectrum of the free ligand exhibits the characteristic bands of two different imines (s, C═N), which appear at 1616 cm^{-1} and 1636 cm^{-1}. The strong absorption peak at 3155 cm^{-1} is due to the imine NH (bending) group, confirming the formation of asymmetric ligand. These observations are consistent with those described in an earlier report.[36]

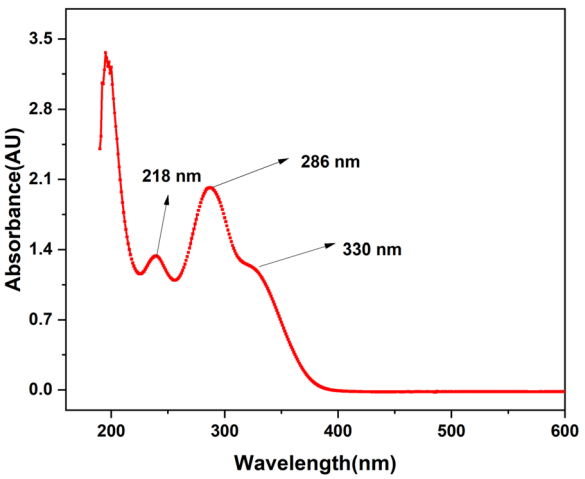

Fig. 1 UV-Visible absorption spectrum for H_2bpabza.

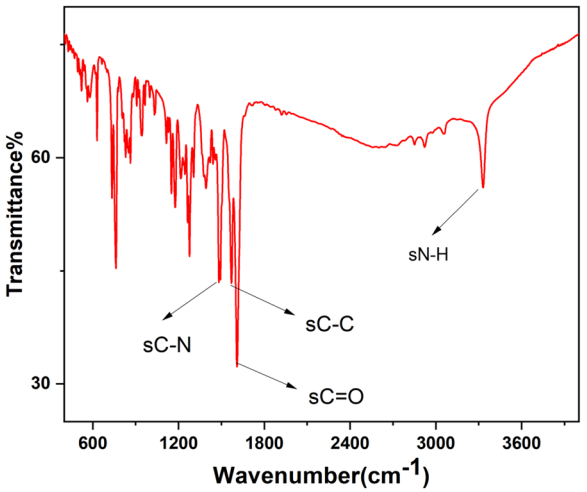

Fig. 2 FT-IR spectrum of H_2bpabza.

3.1.3 Raman spectroscopy. The Raman spectrum of asymmetric ligand is shown in Fig. 3(A) and (B). The Raman spectrum of asymmetric ligand shows absorption corresponding to the

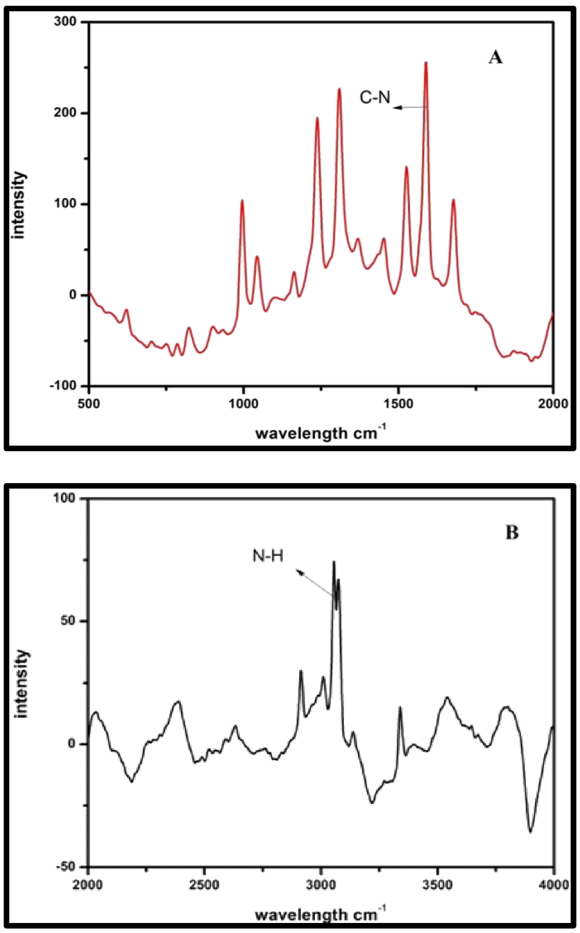

Fig. 3 Confocal Raman spectra of H_2bpabza (A) and (B).

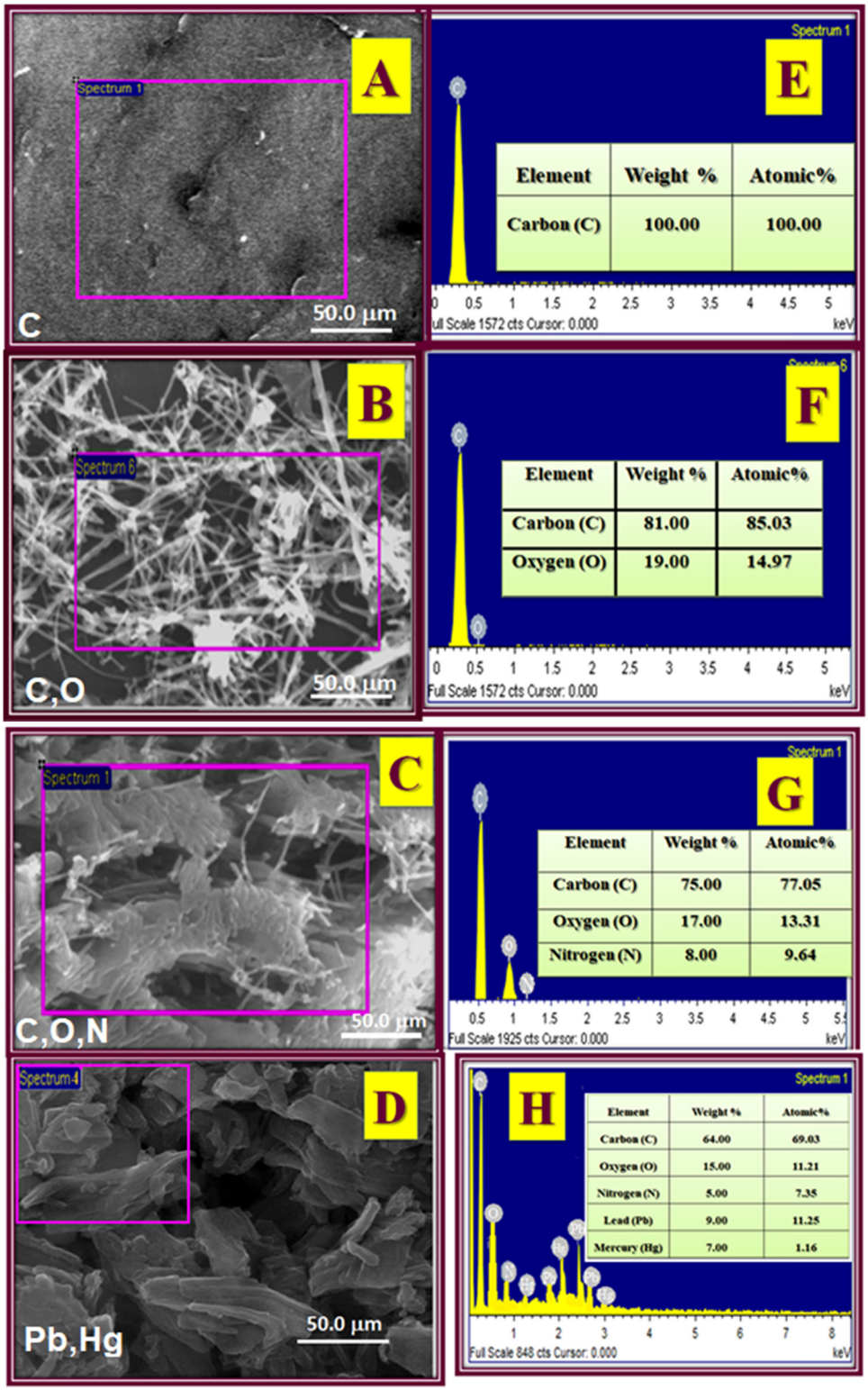

Fig. 4 SEM with EDAX images of (A) and (E) PGE, (B) and (F) MWCNT, (C) and (G) H_2bpabza/MWCNT, and (D) and (H) [Pb^{2+} and Hg^{2+}–H_2bpabza]/MWCNT electrodes.

presence of the free C–N group at 1587 cm^{-1} and the presence of the N–H group at 3056 cm^{-1}, confirming the formation of asymmetric ligand.

3.2. SEM with EDAX

The surface morphologies of the PGEs (unmodified electrode), MWCNT, H_2bpabza/MWCNT, and [Pb^{2+} and Hg^{2+}–H_2bpabza]/MWCNT

(modified PGEs) were confirmed with scanning electron microscopy (SEM) and energy dispersive X-ray (EDAX) spectroscopy. The results of SEM with EDAX for different electrodes are shown in Fig. 4. The morphology of the PGE was observed as a homogeneous dispersed surface in Fig. 4(A), and the EDAX peak was noted as the presence of a carbon element in Fig. 4(E). The MWCNTs appear as needle-like structures (Fig. 4(B)), and the EDAX peak indicates the presence of carbon and oxygen (Fig. 4(F)). In Fig. 4(C), H_2bpabza/MWCNT exhibits a cloudy fibre-like structure, and Fig. 4(G) shows that the EDAX of H_2bpabza/MWCNT contains carbon, oxygen, and nitrogen peaks. The fibre-like structure of [Pb^{2+} and Hg^{2+}–H_2bpabza]/MWCNT is shown in Fig. 4(D), and in Fig. 4(H), the EDAX peak shows the presence of carbon, oxygen, nitrogen, lead, and mercury. It changes due to the chemical reactions leading to different SEM morphologies.

3.3. Cyclic voltammetry and electrochemical impedance spectroscopy

The elaborated H_2bpabza/MWCNT, PGE, and MWCNT electrodes were electrochemically characterized using cyclic voltammetry (CV) and electrochemical impedance spectroscopy (EIS) in 5 mM of $K_4Fe[CN]^{2-/3-}$ and 0.1 M acetate buffer solution (ABS) at a scan rate of 50 mV s^{-1}. The cyclic voltammetry for the H_2bpabza/MWCNT, PGE, and MWCNT electrodes is depicted in Fig. 5(A). The separation of the anodic and cathodic peak potential of ΔE_p and also the ratio of peak current densities (I_{pa}/I_{pc}) between the anodic peak current (I_{pa}) and cathodic peak current (I_{pc}) values are evaluated in Table 2. After electrode modification, there was a clear tendency towards a reversible redox probe when MWCNTs were drop-cast with the H_2bpabza ligand. Additionally, there was a poor redox peak for the PGE and MWCNT electrode.

To increase our understanding regarding the information acquired from CV curves, EIS was carried out. The electron transfer capacity on the surface of the MWCNT electrode was examined using EIS before and after its modification. The Nyquist plot in Fig. 5(B) demonstrates a semicircle in the lower frequency region for each electrode. The small semicircle of the MWCNTs is equivalent to a charge transfer resistance (R_{ct}) equal to 230 ohms. The addition of H_2bpabza to the MWCNT electrode reduced the semicircle diameter and decreased R_{ct} to 133 ohms. In the case of the PGE, the R_{ct} was estimated as 7250 ohms. This can be justified by the change in the electrochemical characteristics of the surface electrodes, which positively affected the electron transfer process. These results prove that the charge transfer of H_2bpabza/MWCNT is faster than that of the MWCNT electrode. Hence, CV and EIS support the successful fabrication and excellent performance of H_2bpabza/MWCNT.

3.4 Voltammetry analysis of $Pb^{2+}$and Hg^{2+}

Although a number of reports on the determination of $Pb^{2+}$and Hg^{2+} by anodic stripping voltammetry using different mercury-based electrodes can be found in the literature, the toxicity and associated health hazards surrounding mercury can be avoided by developing mercury-free electrodes for anodic stripping analysis. Preliminary investigation with the H_2bpabza/MWCNT-modified electrode showed that the Schiff base ligand is a potential complexing agent and can be used for the preconcentration of Pb^{2+} and Hg^{2+}. Hence, various parameters that can influence the anodic stripping voltammetric determination of Pb^{2+} and Hg^{2+} such as medium for complexation, pH, preconcentration time, and reduction potential have been optimized.

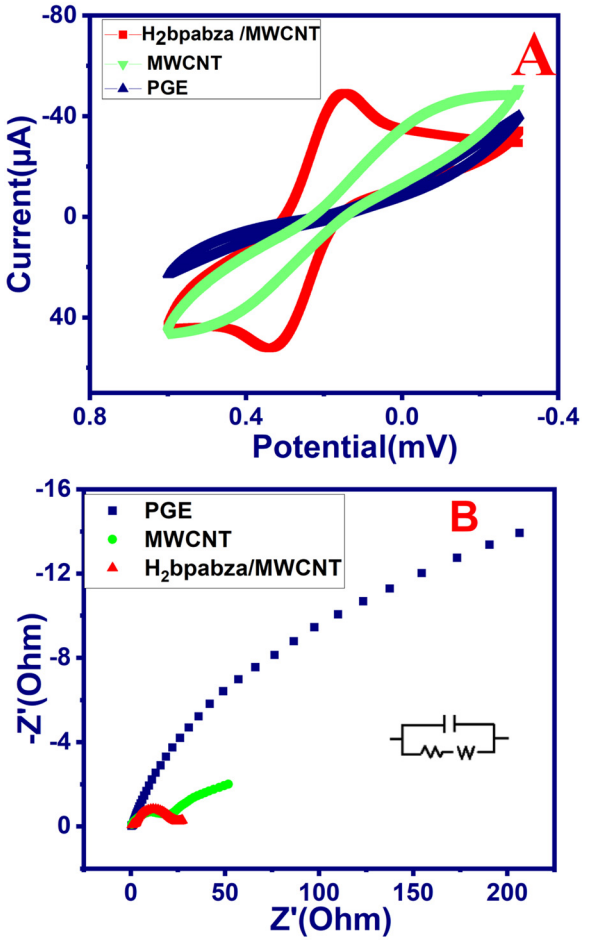

Fig. 5 Electrochemical characterization for H_2bpabza/MWCNT: (A) cyclic voltammetry (CV) and (B) EIS for $Fe(CN)_6^{2-/3-}$ containing 0.1 M acetate buffer, scan rate: 50 mV s^{-1}.

3.4.1. Standard procedure for measurement. The determination of Pb^{2+} and Hg^{2+} was performed as per the following procedure (Scheme 2):

Step 1: Pb^{2+} and Hg^{2+} ions were first preconcentrated by immersing the modified electrode into 0.1 M acetate buffer (pH 4.5) containing Pb^{2+} and Hg^{2+} under open circuit conditions (OCC) for 180 s to form complexes with the H_2bpabza ligand.

$$[M^{2+}]_{solution} + (H_2bpabza/MWCNT)_{surface} \rightarrow (M^{2+} - H_2bpabza/MWCNT)_{surface}$$

Step 2: a potential of −0.8 V in 0.1 M acetate buffer was applied for the reduction of (M^{2+} to M^0).

$$(M^{2+} - H_2bpabza/MWCNT)_{surface} + 2e^- \rightarrow (M^0 - H_2bpabza/MWCNT)_{surface}$$

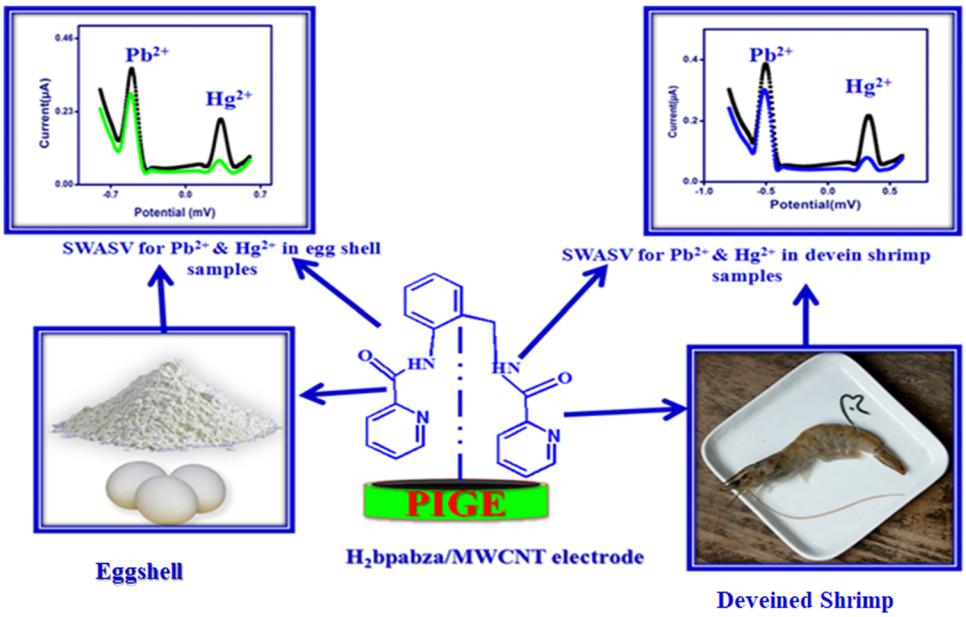

Scheme 2 Mechanism of the H_2bpabza/MWCNT electrode for detection of Pb^{2+} and Hg^{2+}.

Step 3: the metal present on the electrode surface was anodically stripped by scanning the potential from −0.8 V to 0.6 V using square wave anodic stripping with optimized parameters (frequency 25 Hz; amplitude 25 mV; increment potential 4 mV).

$$(M^0 - H_2bpabza/MWCNT)_{surface} \rightarrow H_2bpabza/MWCNT_{surface} + [M^{2+}]_{solution} + 2e^-$$

The metal ions on the electrode surface were removed by dipping in 0.1 M EDTA solution for 60 s with stirring. The metal ions from the electrode surface are introduced into solution *via* EDTA, and then form a complex with EDTA-M^{2+} at pH 4.5. Then, the H_2bpabza/MWCNT-modified electrode was completely washed with distilled water to regenerate it for further experiments. The results obtained are shown in Fig. 6. The above procedure was applied for the MWCNT and H_2bpabza/MWCNT electrodes.

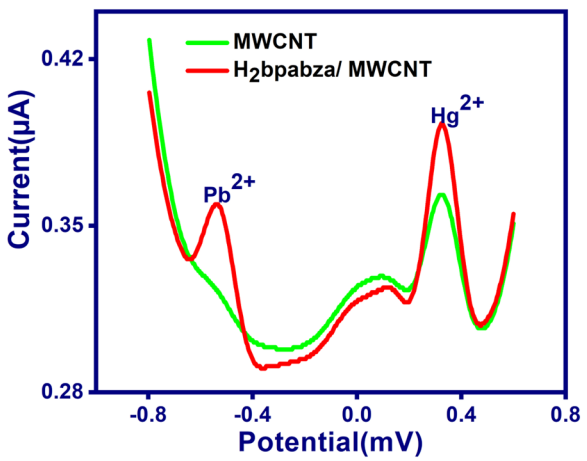

Fig. 6 SWASV for 90 μg L^{-1} of Pb^{2+} and Hg^{2+} on the MWCNT and H_2bpabza/MWCNT-modified electrodes in 0.1 M acetate buffer, pH 4.5. Scan rate: 50 mV s^{-1}.

3.5. Studies on experimental variables for the anodic stripping voltammetry of Pb^{2+} and Hg^{2+}

To increase the sensitivity for the determination of Pb^{2+} and Hg^{2+} with the H_2bpabza/MWCNT electrode, different experimental conditions for SWASV were optimized such as the supporting electrolyte, pH, and preconcentration time.

3.5.1. Medium for preconcentration. Experiments were carried out with 0.1 M solutions of acetate buffer, KNO_3, H_2SO_4, $NaNO_3$, and NH_4NO_3 for the determination of 50 μg L^{-1} Pb^{2+} and Hg^{2+} by SWASV. The pH was adjusted to 4.5 for complexation. A maximum stripping peak current was observed when 0.1 M acetate buffer solution was used as the medium for preconcentration (Fig. 7(A)). Thus, for higher sensitivity for Pb^{2+} and Hg^{2+} determination with the modified electrode, acetate buffer medium was chosen as the electrolyte for preconcentration.

3.5.2. Effect of pH. The effects of pH on the stripping analysis of the modified electrode for the determination of Pb^{2+} and Hg^{2+} were also investigated by SWASV in 0.1 M acetate buffer solution containing 50 μg L^{-1} of Pb^{2+} and Hg^{2+} under open-circuit conditions. The sensitivity of the anodic stripping voltammetric (ASV) analysis of metal ions through complexation with the chelating ligand is strongly dependent upon the pH and the nature of the medium. The electrochemical response of the modified electrode towards the detection of Pb^{2+} and Hg^{2+} was initially studied by SWASV at different pH values using acetate buffer solution. The variations in the anodic stripping current response to Pb^{2+} and Hg^{2+} with respect to solution pH

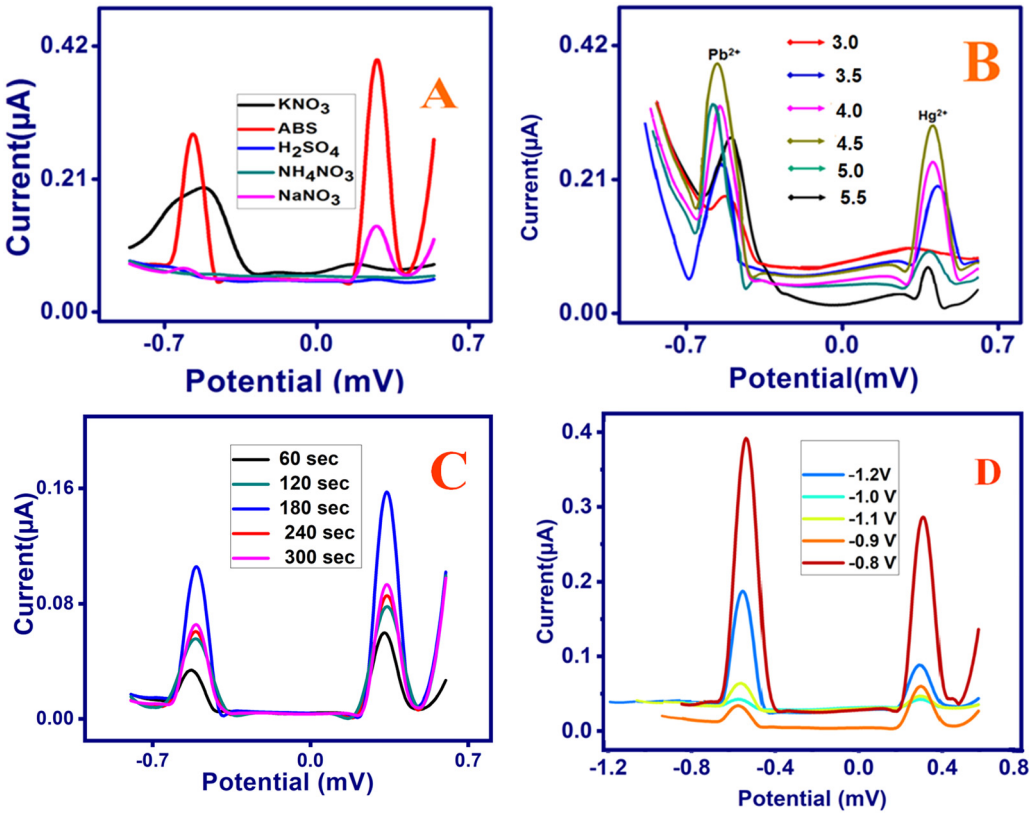

Fig. 7 Optimization of experimental conditions. Influence of (A) supporting electrolytes, (B) pH, (C) deposition time, and (D) deposition potential on the voltammetric response of the H_2bpabza/MWCNT-modified electrode for 50 μg L^{-1} of Pb^{2+} and Hg^{2+}, deposition potential: −0.8 V, frequency 25 Hz; amplitude, 25 mV; increment potential 4 mV.

are shown in Fig. 7(B). The stripping peak current increases with increasing pH of the medium from 3.0 to 4.5, and then decreases with further increasing of the pH. Therefore, pH 4.5 was chosen as the optimum pH for the preconcentration of metal ion on the H_2bpabza/MWCNT electrode.

3.5.3. Effect of preconcentration time. The effect of preconcentration time on the stripping analysis for the determination of Pb^{2+} and Hg^{2+} with the modified electrode was also investigated by SWASV in 0.1 M acetate buffer solution at pH 4.5 containing 50 μg L^{-1} of Pb^{2+} and Hg^{2+} under open-circuit conditions. The variations in the anodic stripping peak current of Pb^{2+} and Hg^{2+} with respect to the change in the preconcentration time in the range from 60 to 360 s are shown in Fig. 7(C). The stripping peak current sharply increases within the first 180 s, and then a constant current is reached, which suggests that the preconcentration of Pb^{2+} and Hg^{2+} at the H_2bpabza/MWCNT-modified electrode reaches saturation after 180 s. After accounting for sensitivity and efficiency, a preconcentration period of 180 s was chosen for the other experiments.

3.5.4 Effect of deposition potential. SWASV evaluated the effect of varied deposition potentials on Pb^{2+} and Hg^{2+} stripping using the H_2bpabza/MWCNT-modified electrode in a 0.1 M acetate buffer solution with a pH of 4.5 and 50 μg L^{-1} of Pb^{2+} and Hg^{2+} under open-circuit conditions. The deposition potential changes from −1.2 V to −1.1 V, −1.0 V, 0.9 V, and 0.8 V in Fig. 7(D), which shows the different anodic stripping peak currents of Pb^{2+} and Hg^{2+}. As shown in Fig. 7(D), the stripping peak current quickly increases at −0.8 V and then decreases from −0.9 V to −1.2 V, showing that the deposition potential of Pb^{2+} and Hg^{2+} at the H_2bpabza/MWCNT-modified electrode decreases after −0.8 V. As a result, a deposition potential of −0.8 V was used for subsequent steps.

3.6. Calibration data

Under optimal conditions, the H_2bpabza/MWCNT-modified electrode was applied for the determination of Pb^{2+} and Hg^{2+} in 0.1 M acetate buffer solution. The SWASV response towards Pb^{2+} and Hg^{2+} at different concentrations was measured by preconcentrating the metal ions for 180 s on the electrode surface in 0.1 M acetate buffer at pH 4.5. The electrode was then removed from the metal ion solution, washed, stored in fresh background electrolyte of acetate buffer, subsequently reduced at −0.8 V, and then, SWASV was recorded. The SWASV responses of Pb^{2+} and Hg^{2+} at different concentrations ranging from 2 to 140 μg L^{-1} are shown in Fig. 8(A). The stripping peak current was linear with increasing concentration of the metal ion. The correlation equations were defined as $Y = 0.005x + 3.31$ μg L^{-1}, $R^2 = 0.98$; $Y = 0.005x + 3.221$ μg L^{-1}, $R^2 = 0.99$ for Pb^{2+} and Hg^{2+}, respectively (Y: current/μA, x: concentration/μg L^{-1}), and the calibration curves are shown in Fig. 8(B). The limit of detection (LOD) was found to be 0.1 and 0.3 μg L^{-1} for Pb^{2+} and Hg^{2+}, respectively. The results indicate that the proposed

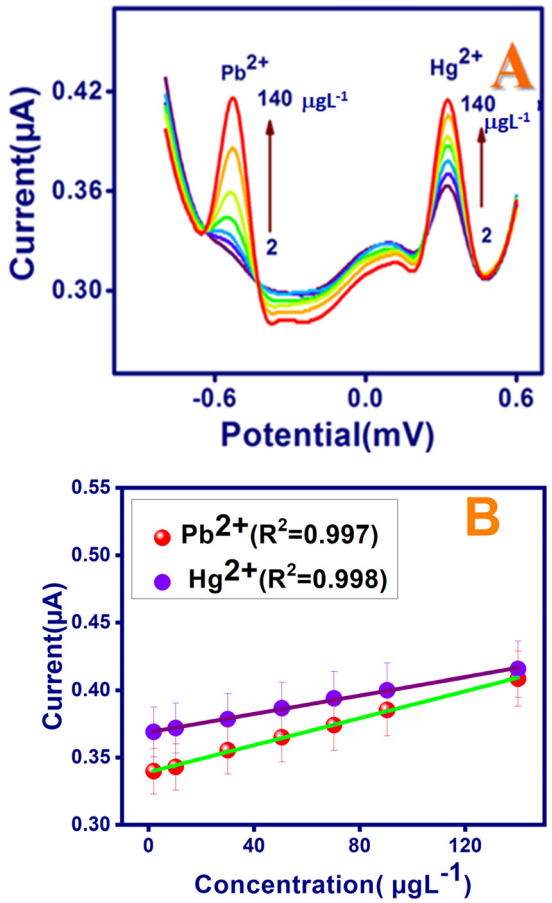

Fig. 8 (A) SWASV responses and (B) the corresponding calibration plot of the H_2bpabza/MWCNT electrode in the detection of Pb^{2+} and Hg^{2+} over a concentration range of 2, 10.3, 30, 50.3, 70.3, 90.4, and 140 µg L^{-1} for Pb^{2+} and Hg^{2+} by deposition for 180 s in 0.1 M acetate buffer (pH 4.5). Deposition potential: −0.8 V; frequency 25 Hz; amplitude 25 mV; increment potential 4 mV.

method shows high sensitivity for the detection of heavy metals. Furthermore, Table 1 shows that the H_2bpabza/MWCNT-modified electrode exceeded previously reported modified electrodes in terms of linear range and detection limits. The table clearly shows that the proposed technique performs at or is comparable to the previously described methods in terms of detection limit and linearity range.

3.7. Reproducibility, stability, and reusability

The H_2bpabza/MWCNT electrode exhibited long-term stability with no systematic differences in performance between the freshly prepared electrodes and electrodes stored for 3 weeks after preparation, in SWASV experiments with 40 µg L^{-1} for Pb^{2+} and Hg^{2+}, as Fig. 9(A) shows no significant change in the current response. Fig. 9(B) shows the reproducibility of five H_2bpabza/MWCNT electrodes produced in 0.1 M acetate buffer with 40 µg L^{-1} of Pb^{2+} and Hg^{2+}. There was satisfactory reproducibility, with a relative standard deviation (RSD) of 3.1% and 2.8% for Pb^{2+} and Hg^{2+} ions, respectively. The reusability of H_2bpabza/MWCNT was analysed each day, up to six days, to detect the stripping peak current of Pb^{2+} and Hg^{2+}, as shown in Fig. 9(C). Excellent reusability of the H_2bpabza/MWCNT electrode was noted, with an RSD value of 1.5% for Pb^{2+} and 1.4% for Hg^{2+} ions. Therefore, the prepared electrode exhibits excellent stability, reproducibility, and reusability for the determination of Pb^{2+} and Hg^{2+} ions.

3.8. Anti-interference studies

Anti-interference was performed to analyze the selectivity and feasible interference of the H_2bpabza/MWCNT-modified electrode for the detection of Pb^{2+} and Hg^{2+} ions. The measurement was examined using SWASV analysis in 0.1 M acetate buffer solution (pH 4.5) containing 90 µg L^{-1} Pb^{2+} and Hg^{2+} with the addition of 50 µg L^{-1} of feasible interference ions of Cu^{2+}, Cd^{2+}, Zn^{2+}, Sn^{2+}, Fe^{2+}, Ni^{2+}, Mn^{2+}, and Co^{2+} (Fig. 10). According to eqn (1), the stripping peak currents of Pb^{2+} and Hg^{2+} in the absence (I_0) and presence (I_i) of interfering metal ions, and the relative signal changes, were calculated in Table 3. Using the equation, the RSD values were evaluated from Table 3. The results obtained from Table 3 show that the peak currents of Pb^{2+} in the presence of interfering metals Cu^{2+}, Cd^{2+}, Zn^{2+}, Sn^{2+}, Fe^{2+}, Ni^{2+}, Mn^{2+}, and Co^{2+} endured a minimal decrease, with RSD% values of 1.05% (Co^{2+}, Cu^{2+}, Zn^{2+}), 1.03% (Mn^{2+}), and 1.31% (Cd^{2+}, Sn^{2+}, Fe^{2+}, Ni^{2+}). For the Hg^{2+} ion, interfering with Cu^{2+}, Cd^{2+}, Zn^{2+}, Sn^{2+}, Fe^{2+}, Ni^{2+}, Mn^{2+}, and Co^{2+} resulted

Table 1 Comparison by SWASV of various modified electrodes for Pb^{2+} and Hg^{2+} detection

Modified electrode	LOD Pb^{2+} µg L^{-1}	LOD Hg^{2+} µg L^{-1}	Linear range of Pb^{2+} µg L^{-1}	Linear range of Hg^{2+} µg L^{-1}	Ref.
Hg-Bi/PDAAQ/GC	3.8	—	10.0–120.0	—	38
3D printed graphene/poly(lactic acid) (PLA)	4.1	6.1	16–10	0–120	39
Hg/GCE, Au & dual-channel	0.05	—	0.10–80	—	40
Ca-MOF/3D printer	—	0.6	—	2–40	41
MMT-Ca/CPE	105	540	3500–15 000	1000–10 000	42
AuNP/0.75% APTES-ITO	0.9	—	5–120	—	43
Bi-BDC-NH_2@NMCS	0.36	—	1.0–1500	—	44
rGO/MoS_2/CS	1.6		5–50	—	45
Eu_{3+} doped NiO/CPE	0.1	—	0.8–165	—	46
Fe_3O_4@MPC-1	34.2	19.3	0.2–1.0	1.0–4.0	47
CuONPs/PANI–CPE	0.40	0.66	0.2–7.8	0.2–7.8	48
COFS-CH_3-modified CPE	0.01	—	0.1–1.0	—	49
SNW_1/GCE	7.2	1.2	10–300	50–300	50
H_2bpabza/MWCNT	0.1	0.3	2–140	2–140	This work

Table 2 Cyclic voltammetry and electrochemical impedance spectroscopy for MWCNT and H_2bpabza/MWCNT

		Modified electrode		
Technique	Term	PGE	MWCNT	H_2bpabza/MWCNT
CV	I_{pa} (μA)	13.8	38.5	51.5
	ΔE_p	90 mV	174 mV	253 mV
	σ	163 × 10^{-5} S cm^{-1}	400 × 10^{-5} S cm^{-1}	515 × 10^{-5} S cm^{-1}
	A (cm^2)	0.14	0.2	0.6
EIS	R_S (Ω)	18	25	40
	R_{CT} (Ω)	7250	230	133

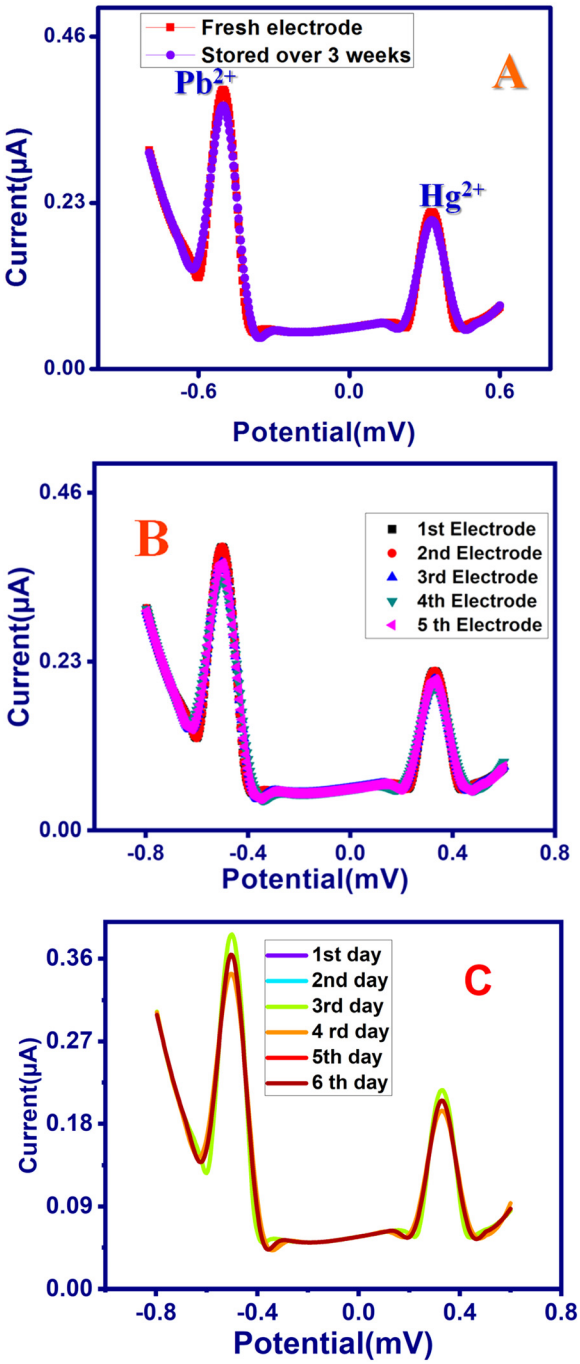

Fig. 9 SWASV for H_2bpabza/MWCNT: (A) stability of fresh electrodes and electrodes stored for 3 weeks and (B) reproducibility for different electrodes. (C) Reusability in 0.1 M acetate buffer for 90 μg L^{-1} Pb^{2+} and Hg^{2+} at a scan rate of 50 mV s^{-1}.

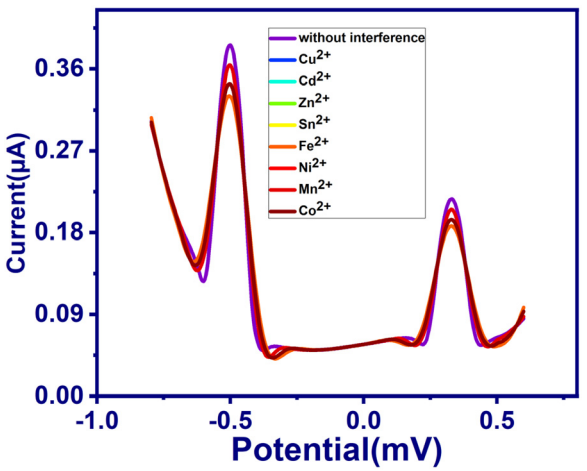

Fig. 10 SWASV of H_2bpabza/MWCNT in 0.1 M acetate buffer containing 90 μg L^{-1} Pb^{2+} and Hg^{2+} with the addition of 50 μg L^{-1} Cu^{2+}, Cd^{2+}, Zn^{2+}, Sn^{2+}, Fe^{2+}, Ni^{2+}, Mn^{2+}, and Co^{2+} at a scan rate of 50 mV s^{-1}.

Table 3 Selectivity interference of Cu^{2+}, Cd^{2+}, Zn^{2+}, Sn^{2+}, Fe^{2+}on Pb^{2+}& Hg^{2+} detections

	Peak current (μA)		Relative signals changes (%)	
Interference	Pb^{2+}	Hg^{2+}	Pb^{2+}	Hg^{2+}
No interference	0.38	0.22	—	—
Cu^{2+}	0.34	0.20	−1.05	−0.9
Cd^{2+}	0.33	0.19	−1.31	−0.81
Zn^{2+}	0.34	0.20	−1.05	−0.9
Sn^{2+}	0.33	0.187	−1.31	−0.81
Fe^{2+}	0.33	0.185	−1.31	−0.812
Ni^{2+}	0.33	0.185	−1.31	−0.81
Mn^{2+}	0.35	0.21	−1.03	−0.95
Co^{2+}	0.34	0.20	−1.05	−0.9

in RSD% value decreases of 0.9% (Co^{2+}, Cu^{2+}, Zn^{2+}), 0.81% (Cd^{2+}, Sn^{2+}, Ni^{2+}), 0.81% (Fe^{2+}), and 0.95% (Mn^{2+}). This can be explained by the presence of several metal ions between the analytes Pb^{2+} and Hg^{2+}, which interfered with Cu^{2+}, Cd^{2+}, Zn^{2+}, Sn^{2+}, Fe^{2+}, Ni^{2+}, Mn^{2+}, and Co^{2+} at the active sites on the H_2bpabza/MWCNT electrode surface. This might be qualified as the result of different metals between the analytes Pb^{2+} and Cd^{2+}, and these interfering Cu^{2+}, Cd^{2+}, Zn^{2+}, Sn^{2+}, Fe^{2+}, Ni^{2+}, Mn^{2+}, and Co^{2+} ions on the active sites are present on the H_2bpabza/MWCNT electrode surface [48].

$$RSD = (I_i/I_0) - 1 \quad (1)$$

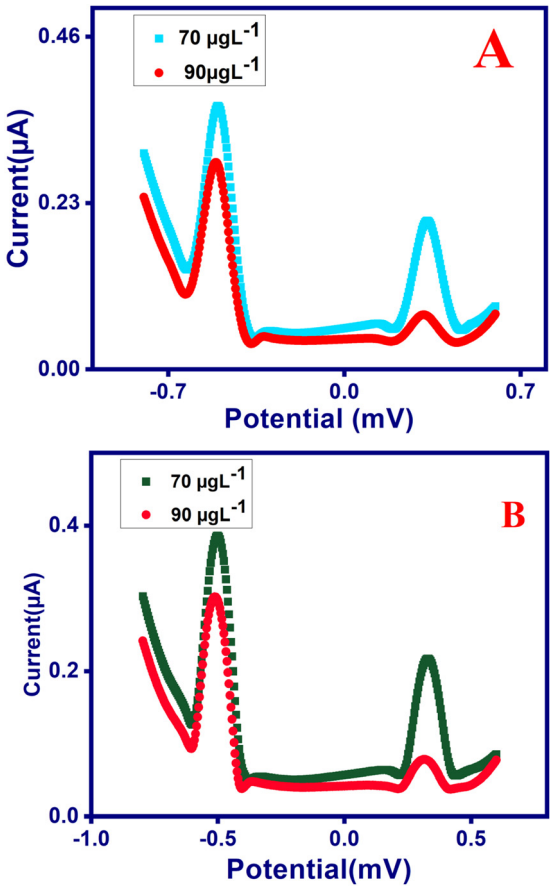

Fig. 11 Stripping analysis of Pb^{2+} and Hg^{2+} (70 and 90 µg L^{-1}, respectively) in (A) deveined shrimp and (B) eggshell samples on the H_2bpabza/MWCNT electrode in 0.1 M acetate buffer. Scan rate: 50 mV s^{-1}.

3.9. Real samples

The H_2bpabza/MWCNT was evaluated by measuring Pb^{2+} and Hg^{2+} in sample A (deveined shrimp) and sample B (eggshells) by SWASV. First, 1 g each of deveined shrimp and eggshells was diluted three times in 0.1 M acetate buffer at pH 4.5. The samples were also diluted three times for analysis of 70 to 90 µg L^{-1} of Pb^{2+} and Hg^{2+}. The SWASV for determination of Pb^{2+} and Hg^{2+} in deveined shrimp (Fig. 11(A)) and eggshells (Fig. 11(B)), and the recovery % of the diluted (deveined shrimp and eggshell) samples are demonstrated in Table 4. The samples showed a superior recovery value of 99% to 101% for Pb^{2+} and 101% to 103% for Hg^{2+}. The prepared H_2bpabza/MWCNT electrode exhibited satisfactory accuracy (recovery) for the detection of Pb^{2+} and Hg^{2+} in the samples of deveined shrimp and eggshells.

Table 4 Recoveries of Pb^{2+} and Hg^{2+} in Devein Shrimp and Egg Shell

	Added (µg L^{-1})		Found (µg L^{-1})		Recovery (%)	
Sample	Pb^{2+}	Hg^{2+}	Pb^{2+}	Hg^{2+}	Pb^{2+}	Hg^{2+}
Blank	0	0	0.100	0.101	100	101
Deveined	70	70	70.1 ± 0.01	71.0 ± 0.04	100	101
shrimp	90	90	90.5 ± 0.02	91 ± 0.01	101	101
Blank	0	0	0.100	0.101	100	101
Egg shell	70	70	69.8 ± 0.03	71.8 ± 0.01	100	103
	90	90	89.5 ± 0.01	91.5 ± 0.02	99	102

4. Conclusions

In this work, a simple, reproducible, and sensitive procedure was developed for the simultaneous determination of Pb^{2+} and Hg^{2+} ions using an H_2bpabza/MWCNT ligand-modified electrode. The results suggest that Schiff base ligand is a promising material that possesses advantages for stripping analysis in comparison with other suggested electrodes for detecting Pb^{2+} and Hg^{2+} ions with detection limits in the range of 0.1 µg L^{-1} and 0.6 µg L^{-1}, with high sensitivity and long-term usage. It was found that operational parameters such as pH, deposition time, and supporting electrolyte systematically affected the stripping current. The H_2bpabza/MWCNT-modified electrode showed satisfactory selectivity, stability, and reproducibility.

Data availability

Data files can be shared on reasonable request.

Conflicts of interest

There are no conflicts to declare.

Acknowledgements

Thanks for providing laboratory facilities to carry our research work. There is no fund provided any of the our institutions for this research work. We have spent our own money for all the characterization studies.

References

1 K. Raj and A. P. Das, Lead pollution: Impact on environment and human health and approach for a sustainable solution, *Environ. Chem. Ecotoxicol.*, 2023, **5**, 79–85.
2 G. de Paula Arrifano, *et al.*, Neurotoxicity and the global worst pollutants: astroglial involvement in arsenic, lead, and mercury intoxication, *Neurochem. Res.*, 2023, **48**(4), 1047–1065.
3 A. I. Gomez-Delgado, *et al.*, Seasonal variations in mercury, cadmium, lead and arsenic species in Norwegian blue mussels (Mytilus edulis L.)–Assessing the influence of biological and environmental factors, *J. Trace Elem. Med. Biol.*, 2023, **76**, 127110.
4 A. Cuschieri, A. Joseph Ignatius and B. Renald, Effect of Non-essential Heavy Metals on Human Health. Heavy Metals in the Environment: Management Strategies for Global Pollution, *Am. Chem. Soc.*, 2023, 117–133.
5 Mi Ye, *et al.*, Monitoring Hg^{2+} and $MeHg^{+}$ poisoning in living body with an activatable near-infrared II fluorescence probe, *J. Hazard. Mater.*, 2023, **445**, 130612.

6 S. L. C. Ferreira, *et al.*, Application of human health risk indices in assessing contamination from chemical elements in food samples, *TrAC, Trends Anal. Chem.*, 2023, 117281.
7 C. Cao, *et al.*, Zeolites synthesized from industrial and agricultural solid waste and their applications: A review, *J. Environ. Chem. Eng.*, 2023, 110898.
8 S. Nawaz, *et al.*, Effective assessment of biopolymer-based multifunctional sorbents for the remediation of environmentally hazardous contaminants from aqueous solutions, *Chemosphere*, 2023, 138552.
9 Z. M. Karazan and M. Roushani, Selective determination of cadmium and lead ions in different food samples by poly(riboflavin)/carbon black-modified glassy carbon electrode, *Food Chem.*, 2023, **423**, 136283.
10 Z. M. Karazan, M. Roushani and S. J. Hoseini, Simultaneous electrochemical sensing of heavy metal ions (Zn^{2+}, Cd^{2+}, Pb^{2+}, and Hg^{2+}) in food samples using a covalent organic framework/carbon black modified glassy carbon electrode, *Food Chem.*, 2024, (442), 138500.
11 Z. M. Karazan and M. Roushani, Electrochemical determination of mercury ions in different food samples using glassy carbon electrode modified with poly(crocin), *Microchem. J.*, 2023, **195**, 109402.
12 M. Winter, F. Lessmann and V. Harth, A method for reliable quantification of mercury in occupational and environmental medical urine samples by inductively coupled plasma mass spectrometry, *Anal. Methods*, 2023, **15**(16), 2030–2038.
13 M. S. Shushtarian, *et al.*, Speciation of inorganic arsenic by μ-thin-layer chromatography coupled with laser ablation inductively coupled plasma mass spectrometry based on an ion imprinted polymer, *Anal. Methods*, 2024, **16**, 205–213.
14 L. He, *et al.*, Cross double point discharge as enhanced excitation source for highly sensitive determination of arsenic, mercury and lead by optical emission spectrometry., *J. Anal. At. Spectrom.*, 2021, **36**(6), 1193–1200.
15 J.-Y. Cai, *et al.*, One-Pot Pretreatment Coupled to Microplasma Optical Emission Spectrometry for Field and Sensitive Determination of Inorganic Mercury and Methylmercury in Fish, *Anal. Chem.*, 2023, **95**(26), 9813–9821.
16 J. C. García-Mesa, *et al.*, Sensitive determination of mercury by magnetic dispersive solid-phase extraction combined with flow-injection-cold vapour-graphite furnace atomic absorption spectrometry, *J. Anal. At. Spectrom.*, 2021, **36**(5), 892–899.
17 M. Atasoy, Development of a New Sensitive Method for Lead Determination by Platinum-Coated Tungsten-Coil Hydride Generation Atomic Absorption Spectrometry, *ACS Omega*, 2023, **8**(25), 22866–22875.
18 X. Liu, *et al.*, Electrothermal desolvation-enhanced dielectric barrier discharge plasma-induced vapor generation for sensitive determination of antimony by atomic fluorescence spectrometry., *Anal. Chem.*, 2022, **94**((10)), 4455–4462.
19 P. Srinivasan, *et al.*, Chromoionophoric probe imbued porous polymer monolith as a Three-in-One Solid-state Naked-eye sensor for the selective sensing and recovery of Ultra-trace Lead, Mercury, and cadmium ions from Industrial/Environmental samples, *Chem. Eng. J.*, 2023, **471**, 144627.
20 J. Kaur, *et al.*, Fabrication of novel copper MOF nanoparticles for nanozymatic detection of mercury ions, *J. Mater. Res. Technol.*, 2023, **22**, 278–291.
21 D. B. C. Leslee, *et al.*, Synthesis of a quinoxaline–hydrazinobenzothiazole based probe—single point detection of Cu^{2+}, Co^{2+}, Ni^{2+} and Hg^{2+} ions in real water samples, *Org. Biomol. Chem.*, 2023, **21**(19), 4130–4143.
22 Y. Zhang, *et al.*, Xylan derived carbon dots composite ZIF-8 and its immobilized carbon fibers membrane for fluorescence selective detection Cu^{2+} in real samples, *Chem. Eng. J.*, 2023, **474**, 145804.
23 E. Erdemir, *et al.*, Smartphone-assisted dual-channel discriminative detection of Hg(II) and Cu(II) ions with a simple, unique, readily available probe., *Sens. Actuators, B*, 2023, **382**, 133487.
24 J. Gayathri., S. Sivakumar. and S. S. Narayanan, Synthesis and characterization of Schiff base ligand-mutliwalled carbon nanotubes as mercury-free electrochemical sensor for detecting toxic metals in aquatic treatment, *Diamond Relat. Mater.*, 2023, **136**, 109984.
25 S. M. Ghalebi, H. Parham and A. Shirmardi, Hg^{2+} determination by DPASV by using poly(methylene disulfide)/Au nanoparticle/MWCNT modified glassy carbon electrode by differential pulse anodic stripping voltammetry (DPASV) technique, *J. Porous Mater.*, 2023, 1–16.
26 J. Liu, *et al.*, Efficient cobalt hydroxide nanosheets for enhanced electrochemical sensing of Hg(II) ion., *Chemosphere*, 2023, **334**, 139015.
27 Y. Gadel Hak, *et al.*, Nanomaterials-modified disposable electrodes and portable electrochemical systems for heavy metals detection in wastewater streams: A review, *Microchem. J.*, 2023, 109043.
28 J. Zhang, *et al.*, Bioamide-Decorated Polyfluoreneisocyanide: Preparation from Benzoxazine-Isocyanide Mechanochemistry Postmodification and Application as an Active Modifier for Pb^{2+}/NO^{2-} Electrochemical Probing, *ACS Appl. Polym. Mater.*, 2023, **5**(7), 5454–5465.
29 C. Ji, *et al.*, Aptamer–Protein Interactions: From Regulation to Biomolecular Detection, *Chem. Rev.*, 2023, **123**(22), 12471–12506.
30 F. Torres-Rojas, *et al.*, Synergistic effect of electrotrophic perchlorate reducing microorganisms and chemically modified electrodes for enhancing bioelectrochemical perchlorate removal, *Environ. Res.*, 2023, 116442.
31 X. Liang, *et al.*, A novel electrochemical acetaminophen sensor based on multiwalled carbon nanotube and poly(neutral red) modified electrodes with electropolymerization in ternary deep eutectic solvents., *J. Electroanal. Chem.*, 2023, **936**, 117366.
32 N. A. A. Elkanzi, *et al.*, Synthesis, physicochemical properties, biological, molecular docking and DFT investigation of Fe(III), Co(II), Ni(II), Cu(II) and Zn(II) complexes of the 4-[{(5-oxo-4, 5-dihydro-1,3-thiazol-2-yl) hydrazono] methyl} phenyl 4-methylbenzenesulfonate Schiff-base ligand, *Polyhedron*, 2023, **230**, 116219.
33 S. Jos and N. R. Suja, Chiral Schiff base ligands of salicylaldehyde: A versatile tool for medical applications and organic synthesis-A review, *Inorg. Chim. Acta*, 2023, **547**, 121323.

34 S. Arulmozhi, *et al.*, Chemical, Pharmacological, and Theoretical Aspects of Some Transition Metal(II) Complexes Derived from Pyrrole Azine Schiff Base., *ACS Omega*, 2023, **8**(38), 34458–34470.

35 R. Kumar, *et al.*, Recent advances in synthesis of heterocyclic Schiff base transition metal complexes and their antimicrobial activities especially antibacterial and antifungal, *J. Mol. Struct.*, 2023, **1294**, 136346.

36 S. Meghdadi, *et al.*, Direct electrochemical synthesis of copper(II) and zinc(II) complexes of the tetradentate ligand *N*,*N*′-bis (2-pyridinecarboxamide)-2-aminobenzylamine (H_2bpabza). The crystal structures of the ligand and its Cu(II) complex., *Polyhedron*, 2015, **85**, 519–524.

37 J. Gayathri and S. Sivalingam, Determination of Pb^{2+} and Cd^{2+} ions in raw milk, honey and groundnut shell using TSAB/MWCNT, *Mater. Adv.*, 2023, **4**, 2502–2511.

38 K. M. Hassan, *et al.*, Single and simultaneous voltammetric sensing of lead(II), cadmium(II) and zinc(II) using a bimetallic Hg-Bi supported on poly(1, 2-diaminoanthraquinone)/glassy carbon modified electrode, *Sens. Bio-Sens. Res.*, 2020, **29**, 100369.

39 J. G. Walters, *et al.*, Trace analysis of heavy metals (Cd, Pb, Hg) using native and modified 3D printed graphene/poly(lactic acid) composite electrodes, *Electroanalysis*, 2020, **32**(4), 859–866.

40 L. Bu, X. Qingji and M. Hai, Simultaneous sensitive analysis of Cd(II), Pb(II) and As(III) using a dual-channel anodic stripping voltammetry approach, *New J. Chem.*, 2020, **44**(15), 5739–5745.

41 C. Kokkinos, *et al.*, 3D-printed lab-in-a-syringe voltammetric cell based on a working electrode modified with a highly efficient Ca–MOF sorbent for the determination of Hg(II), *Sens. Actuators, B*, 2020, **321**, 128508.

42 A. Moutcine, *et al.*, A novel carbon paste electrode modified by NP-Al_2O_3 for the electrochemical simultaneous detection of Pb(II) and Hg(II), *Diamond Relat. Mater.*, 2020, **104**, 107747.

43 N. Mohamad Nor, *et al.*, Simultaneous Sensing of Cd(II), Pb(II), and Cu(II) Using Gold Nanoparticle-Modified APTES-Functionalized Indium Tin Oxide Electrode: Effect of APTES Concentration, *ACS Omega*, 2023, **8**(19), 16587–16599.

44 Q. Yang, *et al.*, Bismuth Metal–Organic Framework/Carbon Nanosphere Composites for Ultrasensitive Simultaneous Electrochemical Detection of Lead and Cadmium, *ACS Appl. Nano Mater.*, 2023, **6**((9)), 7901–7909.

45 C. Guo, *et al.*, A simple electrochemical sensor based on rGO/MoS_2/CS modified GCE for highly sensitive detection of Pb(II) in tobacco leaves., *RSC Adv.*, 2021, **11**(47), 29590–29597.

46 M. Malakootian, A. Hesam and H. Mahmoudi-Moghaddam, A novel electrochemical sensor based on the modified carbon paste using Eu^{3+} – doped NiO for simultaneous determination of Pb(II) and Cd(II) in food samples, *J. Electroanal. Chem.*, 2020, **876**, 114474.

47 Y. Liu, *et al.*, Interface Co-Assembly Synthesis of Magnetic Fe_3O_4@ mesoporous Carbon for Efficient Electrochemical Detection of Hg(II) and Pb(II), *Adv. Mater. Interfaces*, 2023, **10**(5), 2201631.

48 D. S. B. Ali, *et al.*, Green synthesis of copper oxide nanoparticles using Ficus elastica extract for the electrochemical simultaneous detection of Cd^{2+}, Pb^{2+}, and Hg^{2+}, *RSC Adv.*, 2023, **13**(27), 18734–18747.

49 X. Tang, *et al.*, Thiol-grafted covalent organic framework-based electrochemical platforms for sensitive detection of Hg(II) ions, *Chem. Commun.*, 2023, **59**, 8731–8734.

50 M. R. J. Sarvestani, M. Tayyebeh and A. Abbas, Simultaneous determination of Pb^{2+} and Hg^{2+} at food specimens by a Melamine-based covalent organic framework modified glassy carbon electrode, *Food Chem.*, 2023, **402**, 134246.